Progress In Electromagnetics Research, PIER 37, 79–99, 2002

HIGHER ORDER EMISSION MODEL STUDY OF BI-SINUSOIDAL SURFACE BRIGHTNESS TEMPERATURES

J. T. Johnson

Department of Electrical Engineering and ElectroScience Laboratory
The Ohio State University
205 Dreese Laboratories
2015 Neil Ave., Columbus, OH 43210, USA

Abstract—Models for microwave thermal emission from a rough surface are currently of interest due to the goal of improved sea surface wind vector retrievals from polarimetric brightness temperature measurements. Models based on either a small slope approximation or on a physical optics approach have been proposed and have shown some success in matching observations. Both of these models involve series solutions, but computation of higher order terms typically is difficult, particularly for multi-scale sea surface models. Knowledge of higher order term contributions, however, would assist in understanding the limitations of the low-order methods applied in practice. In this paper, higher order results from both the small slope and physical optics methods are studied and compared for a simple bi-sinusoidal surface model (i.e. height profile $= A\sin(\frac{2\pi x}{P_x})\sin(\frac{2\pi y}{P_y})$, where P_x and P_y are the surface periods in the x and y directions, respectively). Results show both methods to provide good predictions for moderate slope "large scale" surfaces (i.e. periods large compared to the observing electromagnetic wavelength) when shadowing and multiple scattering effects are negligible, while only the small slope theory correctly predicts emission from "small scale" profiles. The influence of both shadowing and multiple scattering effects is examined, and the "binary" shadowing behavior used in the physical optics method is suggested as a source of larger errors observed as shadowing effects increase.

1. INTRODUCTION

Several modeling studies of microwave thermal emission from randomly rough surfaces have been performed in recent decades (see [1–23], among others). Models for predicting rough surface brightness temperatures are critical for interpreting measurements from ground, air, or space based radiometric systems. Rough surface effects are particularly important in observations of the sea, and remote sensing of sea wind speed and direction is directly related to emission properties of the sea rough surface [24–29]. Rough surface effects are also important in remote sensing of soil moisture and sea ice properties. Within the last decade, the use of polarimetric radiometers has become more common, so that models that include prediction of the third and fourth Stokes' emission parameters are of increased interest.

Rough surface emission modeling works have been reported based on a physical or geometrical optics approach (PO/GO) [1, 5–7, 9, 11, 12, 16], a two-scale (or "composite surface") method [2, 3, 13], and a small slope approximation (SSA) [14, 18, 20–23]. Some limited studies with numerically exact models have also been reported [15, 17, 19]. Reference [14] demonstrated that the SPM and SSA theories for emission from a rough surface are in fact identical, so that no restriction on surface heights is required in using the theory as long as surface slopes remain moderate. SPM and SSA studies have primarily used the second order theories, although some results with a third order SSA have been recently described [20, 22]. The majority of PO/GO studies have neglected multiple scattering effects, but references [11, 12] describe a higher order ray-tracing approach that includes some multiple scattering contributions. General results

of these studies show that the PO/GO, two-scale, and SSA theories all predict similar forms for emission from "long wave" components of the sea surface (i.e. those with length scales much greater than the electromagnetic wavelength) [23], while only the SSA (or SPM) and two-scale theories capture the resonant emission effects of short wave components in the surface. The influence of shadowing and multiple scattering effects is generally difficult to estimate from previous results, as well as the rate of convergence in both the SSA and PO/GO theories as higher order SSA series or PO/GO multiple scattering contributions are included. Thus, although the rough surface emission modeling area is becoming quite mature, questions remain regarding the accuracy to be expected from the models available.

To address this issue, a study of the higher order SSA and PO/GO theories is performed in this paper. Numerical implementations of these theories are described that allow arbitrary order SSA calculations and an arbitrary number of multiple scattering contributions in the PO/GO model. Although these numerical codes are relatively efficient, insight into the results obtained is not as readily available as with the lower order analytical SSA and PO models; a simple geometry was therefore chosen for the study to reduce the complexity of the results. A bi-sinusoidal surface provides a simple "single mode" geometry so that the influence of surface length scales can be easily determined, and so that a two-scale approach is unnecessary. The general problem geometry is described in detail in Section 2, and formulation of the higher order theories is reviewed in Section 3. Results will be provided in Section 4 for both "large" and "short" scale surfaces, with comparisons of higher order SSA and PO/GO results illustrated in both cases. The accuracy of the standard low order methods for these cases will also be determined, and the influence of shadowing and multiple scattering effects examined. Although the simple geometry considered does not directly model a multi-scale sea surface, the results to be described do provide insight into the utility of the commonly applied models for sea emission prediction.

2. PROBLEM DEFINITION

The geometry considered in this problem is illustrated in Figure 1, and consists of a radiometer located at polar angle θ and azimuth angle ϕ observing a boundary $z(x, y)$ between free space and a non-magnetic medium with relative permittivity ϵ. To approach a sea emission problem, ϵ is set to an approximate relative permittivity for sea water at 19 GHz $(29.04 + i35.55)$ [30] throughout this paper. The surface profile $z(x, y)$ is a periodic bi-sinusoidal surface with amplitude

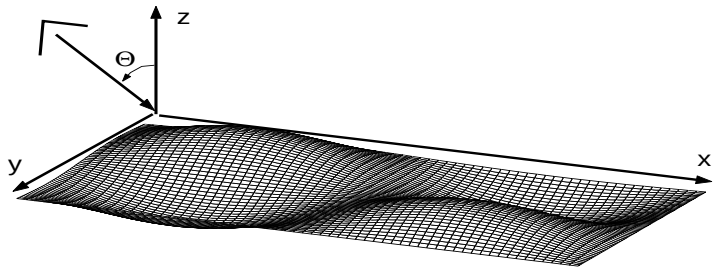

Figure 1. Geometry of problem.

A and periods P_x and P_y:

$$z = A \sin(\frac{2\pi x}{P_x}) \sin(\frac{2\pi y}{P_y}) \tag{1}$$

The radiometer measures the microwave power emitted from this medium in terms of the polarimetric brightness temperature:

$$\bar{T_B} = \begin{bmatrix} T_h \\ T_v \\ U \\ V \end{bmatrix} = T_s \left(\begin{bmatrix} 1 - r_h \\ 1 - r_v \\ -r_U \\ -r_V \end{bmatrix} \right) \tag{2}$$

where T_h and T_v are the brightness temperatures measured by horizontally and vertically polarized antennas, respectively, and U and V are proportional to the real and imaginary parts of the correlation between fields in horizontal and vertical polarizations respectively [10]. The second equality follows from Kirchhoff's Law, which relates the emissivity of a medium at constant temperature to the corresponding reflectivity (r_h, r_v, r_U, and r_V) multiplied with the surface physical temperature T_s (assumed to be 283 K in this paper). Reflectivities in the SSA model are calculated as an integral of bistatic scattering coefficients over the upper hemisphere in the reciprocal active scattering problem [7].

Particular interest in ocean wind remote sensing is given to brightness temperature variations in azimuth, and it is convenient to represent these variations in terms of a set of azimuthal harmonics. Due to the statistical reflection symmetries of the bi-sinusoidal surface about the x and y axes, it can be shown [31] that an appropriate

expansion is

$$\begin{bmatrix} T_h \\ T_v \\ U \\ V \end{bmatrix} \approx \begin{bmatrix} T_h^{\text{flat}} + T_h^{(0)} + T_h^{(2)} \cos 2\phi + \cdots \\ T_v^{\text{flat}} + T_v^{(0)} + T_v^{(2)} \cos 2\phi + \cdots \\ U^{(2)} \sin 2\phi + \cdots \\ V^{(2)} \sin 2\phi + \cdots \end{bmatrix} \tag{3}$$

where ϕ denotes the azimuth angle between the radiometer look direction and the $-\hat{x}$ direction (i.e. $\phi = 0^\circ$ corresponds to a radiometer look direction horizontal component of $-\hat{x}$, while $\phi = 90^\circ$ corresponds to $-\hat{y}$). This paper focuses on the zeroth ($T^{(0)}$) and second ($T^{(2)}$) azimuthal harmonic coefficients that describe the influence of the bi-sinusoidal surface on emitted brightness temperatures. Note that the horizontally and vertically polarized zeroth harmonic coefficients above are defined after the flat surface horizontal and vertical brightnesses (T_h^{flat} and T_v^{flat}, respectively) are subtracted to emphasize the rough surface influence. In the results to be illustrated, zeroth and second azimuthal harmonics are obtained through a least squares fit of equation (3) to brightness temperatures computed at 7 angles in the first quadrant $\phi = 0^\circ$ to $\phi = 90^\circ$. The symmetries of the bi-sinusoidal surface allow results in the remaining three quadrants to be determined from those in the first quadrant alone.

Two particular surface profiles are considered: a "large scale" surface with parameters $P_x = 50.001\lambda$, $P_y = 100.001\lambda$, and amplitude $A = 1.501\lambda$, and a "small scale" surface with parameters $P_x = 2.001\lambda$, $P_y = 4.001\lambda$, and amplitude $A = 0.072\lambda$. These surface periods are chosen as slight deviations from integer values to avoid some numerical complications in the extended boundary condition algorithm to be described in Section 3.3. A ratio of approximately two is chosen between the P_x and P_y values to produce a significant azimuthal asymmetry so that second azimuthal harmonics of brightness temperatures will be obtained. Note that the "small scale" surface is a scaled version of the "large scale" surface, with a scaling factor of approximately twenty five. Both surfaces have only moderate slopes, with a maximum value of approximately 0.19 and an rms slope of 0.149. Geometrical consideration of this surface shows that multiple scattering effects (as defined in [11]) should begin to occur for polar observation angles greater than approximately 68°, while geometric shadowing begins for polar observation angles greater than approximately 79°. Particular attention will therefore be given to emission predictions for angles greater than 65° to examine the influence of multiple scattering and shadowing.

3. EMISSION THEORIES

A brief review of the higher order SSA and PO theories is provided in the following sections, along with a description of the numerical EBC code used to verify predictions in the small scale surface case. Detailed formulations of these methods are available in the references provided in each section.

3.1. Higher Order SSA

Because an SSA theory of emission from a rough surface is identical in form to that from the SPM, a higher order SSA brightness temperature prediction can be obtained by extending the SPM perturbation series for scattering from a rough surface to higher order, and by applying Kirchhoff's law to relate scattering to emission. Analytical SPM forms for scattering from a rough surface typically are reported to second order in surface height [7], but have recently been extended to third order [32, 33]. The third order SPM terms have also been used in deriving analytical SSA expressions for emission from a rough surface at third order [22]. Analytical expressions are highly desirable because they allow insight into the means by which surface properties and emission physics couple to produce observed brightness temperatures. However, analytical determination of higher order SPM terms is extremely tedious, so that extension of analytical expressions to orders beyond third or fourth is not practical.

An alternate approach is available in which higher order SSA terms are determined numerically rather than analytically. An SPM algorithm for this purpose is described in [32], and the higher order mode contributions are easily included in computing brightness temperatures through Kirchhoff's Law. A similar higher order algorithm for scattering from a rough surface is described in [34]. In this method, surface properties and emission physics remain coupled in the results, so that it is not possible to separate the two effects without performing repeated simulations with varying input parameters. A deterministic input surface is also required, sampled into an $N \times N$ set of points, so that averages over a surface stochastic process can be obtained only through Monte Carlo simulations. However, the numerical algorithm is easily extended to arbitrary orders, and is a highly efficient $O(N \log N)$ algorithm that conserves power by definition. One limitation on the SSA order that can be simulated results from the fact that the SPM algorithm at order P involves z^P, so that a sufficient number of points N is required to avoid aliasing effects in z^P. The number of points sampling the surface profile must therefore increase as the desired order increases. Another issue is the precision

required to avoid round-off error as the order increases. For the results to be reported, a quadruple precision implementation was used to insure that roundoff errors remained insignificant. The accuracy of an emission prediction from this approach can be estimated by examining the convergence of the results versus the SSA order considered. Of course, the rate of series convergence is expected to be closely related to the slope of the surface for the small slope approximation; results in Section 4 will examine the error of the second and fourth order SSA as a function of observation angle.

In the results to be illustrated, the bi-sinusoidal surface profile was sampled into 64×64 points, and SSA results were computed up to twentieth order. The "single mode" nature of the bi-sinusoidal surface allows this high order to be achieved without an extremely large number of surface sampling points. The x and y axis symmetries of the bi-sinusoidal surface, along with its symmetry in z, results in no odd order emission contributions. Therefore ten non-zero terms in the correction to flat surface brightness temperatures are available. The computational time required for a single brightness temperature calculation to twentieth order was approximately 45 seconds on an 800 MHz Pentium III processor. Computational time was further reduced for the multiple angles and surfaces of this study through the use of IBM SP parallel computing resources at the Maui High Performance Computing Center [35]. Note that these computational times compare favorably with "exact" numerical algorithms for the rough surface problem [15, 17, 19], while retaining the desirable property of power conservation. A higher order SSA algorithm therefore will likely be the method of choice for obtaining very accurate predictions of emission from Monte Carlo simulations with moderate slope multi-scale ocean surface models.

3.2. Multiple Scattering PO

Standard PO models have been applied in many studies of emission from a rough surface. The basic theory expresses rough surface brightnesses in terms of an integration of "tilted facet" contributions over the slope distribution of the surface. The description of surface features in terms of tilted facets demonstrates that diffraction effects from features comparable to or smaller than the electromagnetic wavelength are not modeled completely, as is typical for any high frequency theory. Previous comparisons of standard PO predictions with other theories have shown this limitation [17]. It has also been shown that SSA and PO predictions are identical for large scale surfaces up to third order in surface slope [23], as long as shadowing and multiple scattering effects are negligible.

Defining the z direction as pointing from the mean surface plane into free space, multiple scattering effects are described as occurring when the specular reflection of a ray from the radiometer to any surface facet has a negative z component, so that the surface will be re-intersected. Local shadowing effects occur when a ray drawn from the radiometer to any surface facet has a local incidence angle greater than 90 degrees, so that the facet is not directly observed. Non-local shadowing occurs when a ray from a surface facet to the radiometer intersects the surface in a second facet. The relative occurrence of these effects generally increases both with the roughness of the surface and with the observation angle.

Estimates of the influence of shadowing and multiple scattering on surface brightness temperatures can be obtained through the use of high frequency "shadowing functions", as described in [9]. However, these functions describe shadowing behaviors only on average, and provide information only on a bound for the influence of these effects. For a deterministic surface, a ray tracing approach can alternatively be used to provide a more specific description of the influence of multiple scattering and non-local shadowing terms. Such a model is described by [11, 12], and is applied in this paper. The model begins with the standard PO contribution for each surface facet, although both local and non-local shadowing are included by neglecting emission from any locally or non-locally (found through a ray tracing algorithm) shadowed facets. Rays from the radiometer to non-shadowed specific facets are then specularly reflected, and any facets intersected by the specularly reflected rays are identified as second order multiple scattering facets. An iterative root finding procedure [36] is used to insure that multiple scattering points on the surface are determined accurately. Emission contributions from the secondary facets are then reflected off the original facet and included in its emission to the radiometer. The process can be continued to an arbitrary order of multiple scattering terms. Emission contributions from multiple scatter facets are not included if any ray to a lower order facet occurs at a local incidence angle greater than 90°. The model is described in detail in [11]; note that the "downwelling" atmospheric brightness temperature used in [11] is set to zero in this study.

Note that the shadowing considered in this approach is described in a binary on/off fashion. Considerable evidence exists (see [37] for example) to suggest that fields in geometrically shadowed regions can make important contributions in scattering and potentially emission problems. Note also that the "multiple scattering PO" theory used for computation of emission here is distinct from recent surface scattering theories based on iteration of the physical optics integral [38–40].

An emission theory based on an accurate iteration of field integral equations would likely be more successful in capturing small scale surface diffraction effects, but also more complex than the higher order physical optics method applied here.

In the results to be illustrated, the bi-sinusoidal surface profile was again sampled into 64×64 points, and multiple scattering contributions included up to fourth order. These multiple scattering contributions began to be observed for both the large and small scale surfaces at polar observation angles greater than approximately 68°, and local and non-local shadowing effects were observed for polar observation angles greater than approximately 79°. The computational time required for a single brightness temperature calculation including fourth order multiple scattering was approximately 1.5 seconds on an 800 MHz Pentium III processor, demonstrating the efficiency of the PO/GO model due to the "tilted facet" approach.

3.3. Extended Boundary Condition Method

A final method was used in the study to verify SSA and PO model predictions in the small scale surface case. The extended boundary condition (EBC) method is a numerically exact approach for determining surface brightness temperatures based on a matrix equation solution of the electromagnetic boundary value problem. The method applied here is described in detail in [15], although some revisions to the algorithm were made to improve efficiency for the bi-sinusoidal surface. In particular, matrix element integrals can be performed analytically in terms of Bessel functions for the bi-sinusoidal surface, as opposed to the facet contribution integration described in [15]. The EBC approach is well known to have conditioning problems for moderate to large slope surfaces, and also with highly lossy media if surface heights are large [41]. The latter restriction prevents the EBC algorithm from being applied for the large scale surface case. In the small scale surface case, a relatively large number of terms in the surface current Fourier series was used to insure accuracy, resulting in a matrix size of 13124×13124. Again, the conditioning problems of the EBC method produce convergence problems with iterative matrix solutions, so a direct solution implemented through the "Scalapack" parallel library [42] was used with Maui High Performance Computing Center SP computer resources. The computational time for a single brightness temperature with 64 computational nodes (each roughly equivalent to a 400 MHz Pentium processor) was approximately eight minutes for each node, illustrating the high computational costs of numerically exact methods. Brightness temperature zeroth and second harmonics in the small scale surface case were found to be

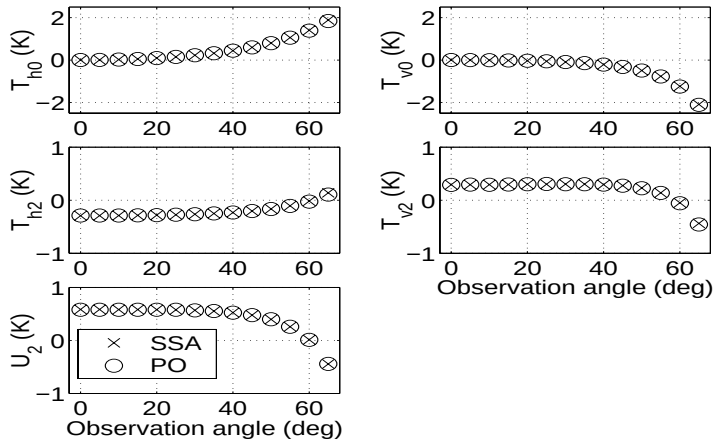

Figure 2. T_{h0}, T_{v0}, T_{h2}, T_{v2}, and U_2 for bi-sinusoidal surface with $A = 1.501\lambda$, $P_x = 50.001\lambda$, and $P_y = 100.001\lambda$ from twentieth order SSA and fourth order PO: $0^\circ < \theta < 65^\circ$.

within 0.01 K of twentieth order SSA results for all polarizations and angles; this level of agreement is within the accuracy expected for EBC results with the specified number of unknowns. A similar level of agreement was observed in the large scale surface case when a surface relative permittivity value of $\epsilon = 3 + i0$ was considered. Because these comparisons indicate that the higher order SSA code is providing accurate predictions for the cases considered, no further reference to EBC results will be described, and twentieth order SSA model predictions will be taken as an accurate description of surface brightness temperatures.

4. RESULTS

Figure 2 plots T_{h0}, T_{v0}, T_{h2}, T_{v2}, and U_2 azimuthal harmonic coefficients versus observation angle from 0 to 65° for the "large scale" surface described in Section 2. V_2 results are not included in this case because of their small amplitude (less than 0.01 K). Results from the twentieth order SSA and the fourth order PO algorithms are compared. For these observation angles, shadowing and multiple scattering contributions are not significant, so higher order PO predictions are identical to those at first order. The plots show a moderate influence of the surface profile on emitted brightness temperatures, with a maximum amplitude of approximately 2 K at the larger observation angles. PO and SSA predictions are in excellent

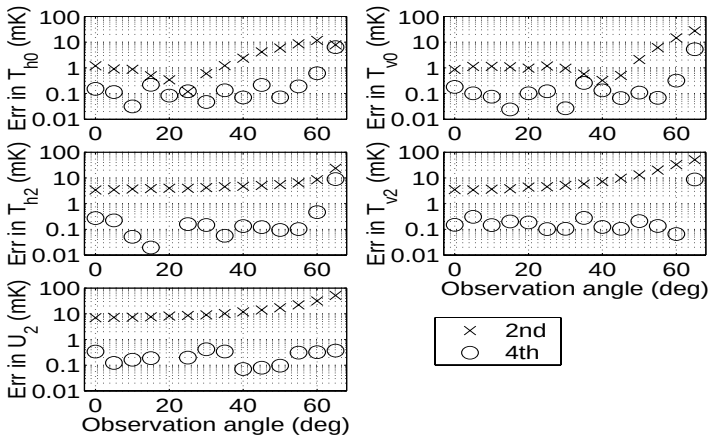

Figure 3. Error in T_{h0}, T_{v0}, T_{h2}, T_{v2}, and U_2 from second and fourth order SSA for bi-sinusoidal surface with $A = 1.501\lambda$, $P_x = 50.001\lambda$, and $P_y = 100.001\lambda$: $0^\circ < \theta < 65^\circ$.

agreement for this case, within the precision of the calculations. The accuracy of second and fourth order SSA predictions is examined in Figure 3, in terms of the absolute value (in milli-Kelvin) of the difference between second or fourth order predictions and those at twentieth order. Results show that the second order SSA is accurate to within 0.05 K for all observation angles considered in the plot, and that the fourth order correction provides improved accuracy. For the observation angles considered in Figure 2, the optical limit is clearly obtained with surface periods of 50.001λ and 100.001λ.

Azimuthal harmonics (including V_2) for the "large scale" surface at observation angles from 65° to 89° are plotted in Figure 4 for the twentieth order SSA and fourth order PO. For the PO calculations in this case, multiple scattering contributions begin to occur for observation angles greater than approximately 68°, and shadowing corrections begin for observation angles greater than approximately 79°. Results show an increased but still moderate influence of the surface profile, with maximum SSA amplitudes of approximately 10 K at the larger observation angles. The accuracy of PO results is found to degrade in this case for observation angles greater than approximately 75°, and to degrade severely for observation angle greater than 80° (many PO values outside Figure limits). As explained in [11], contributions to V_2 in the PO method originate exclusively from multiple scattering terms. Here SSA V_2 harmonics obtain a moderate amplitude for observation angles greater than 70°, but are not captured

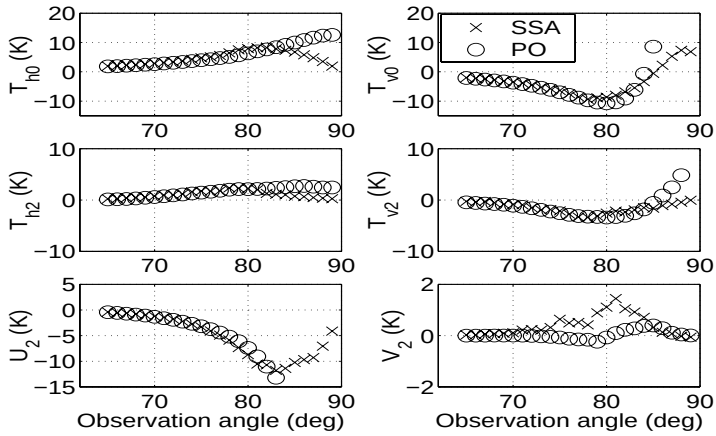

Figure 4. T_{h0}, T_{v0}, T_{h2}, T_{v2}, U_2, and V_2 for bi-sinusoidal surface with $A = 1.501\lambda$, $P_x = 50.001\lambda$, and $P_y = 100.001\lambda$ from twentieth order SSA and fourth order PO: $65^\circ < \theta < 89^\circ$.

accurately by the PO theory. SSA harmonic amplitudes generally show a decreasing trend in all polarizations as grazing is approached, with the exception of T_{v0}. Absolute errors in the second and fourth order SSA are illustrated in Figure 5, and demonstrate a maximum error of approximately 3 K at the larger observation angles in second order predictions. Fourth order predictions are observed to improve accuracy at some angles and to worsen accuracy at others, and the level of increased accuracy when applicable is not as dramatic as that observed in Figure 3. The level of error in first and second order PO predictions (compared to the twentieth order SSA) is illustrated in Figure 6. The larger errors observed in Figure 4 are reproduced here, but improvements in PO predictions from first to second order (i.e. as some multiple scattering contributions are included) are observed for observation angles from approximately 70° to 80°, with the exception of U_2. These results demonstrate that the procedure for including multiple scattering contribution described in [11] indeed captures some of these effects to produce improved accuracy, but also that shadowing effects not captured accurately by the method eventually become problematic. Both SSA and PO results suggest that increased multiple scattering and shadowing effects play a role in convergence of both algorithms.

Figure 7 illustrates the same azimuthal harmonics in the "small scale" surface case described in Section 2 for observation angles from 0° to 55°. In this small scale case, the second order SSA theory

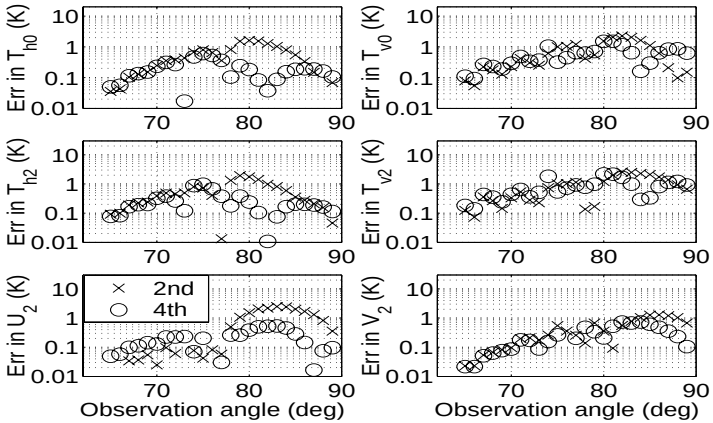

Figure 5. Error in T_{h0}, T_{v0}, T_{h2}, T_{v2}, U_2, and V_2 from second and fourth order SSA for bi-sinusoidal surface with $A = 1.501\lambda$, $P_x = 50.001\lambda$, and $P_y = 100.001\lambda$: $65^\circ < \theta < 89^\circ$.

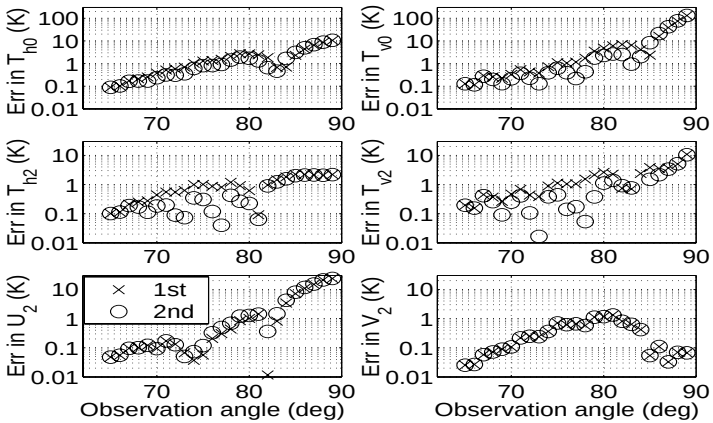

Figure 6. Error in T_{h0}, T_{v0}, T_{h2}, T_{v2}, U_2, and V_2 from first and second order PO for bi-sinusoidal surface with $A = 1.501\lambda$, $P_x = 50.001\lambda$, and $P_y = 100.001\lambda$: $65^\circ < \theta < 89^\circ$.

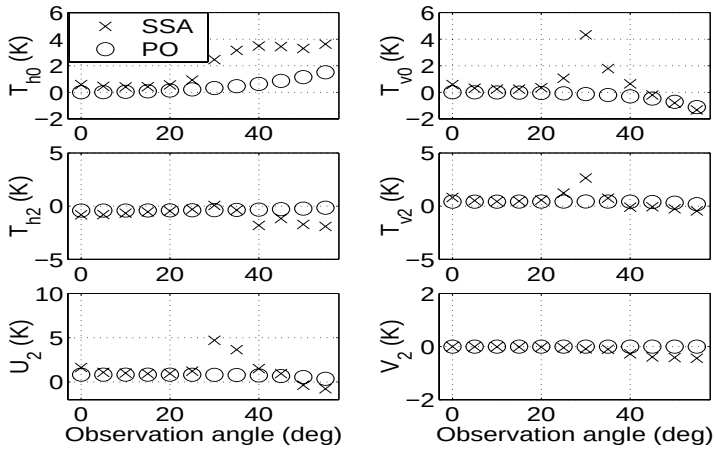

Figure 7. T_{h0}, T_{v0}, T_{h2}, T_{v2}, U_2, and V_2 for bi-sinusoidal surface with $A = 0.072\lambda$, $P_x = 2.001\lambda$, and $P_y = 4.001\lambda$ from twentieth order SSA and fourth order PO: $0° < \theta < 55°$.

predicts potential "critical phenomena" [4] that can occur to produce rapid changes in brightness temperatures versus angle. The results of Figure 7 illustrate such behaviors for observation angles around 30°. Here the effect of the surface profile becomes more significant than in the "large scale" surface case, even though the profiles are identical after a scale factor of approximately 25 is applied. Results show the SSA and PO theories to yield similar (small) predictions for observation angles less than 30°, but significant differences are observed for larger angles due to the neglect of diffraction effects in the PO theory. Absolute errors in the second and fourth order SSA predictions plotted in Figure 8 show inaccuracies of up to 1 K from second order results, improved to 0.1 K maximum at fourth order. Critical phenomenon effects at $\theta = 30°$ play only a minor role in the errors observed.

Similar results are observed for the "small scale" surface at observation angles from 60° to 88° in Figures 9 and 10. Harmonic amplitudes in Figure 9 again show only moderate levels, and also show dramatic errors in PO predictions particularly for observation angles greater than 80°. Absolute errors of second and fourth order SSA results in Figure 10 show similar levels to those of Figure 8 and again indicate a significant improvement when the fourth order theory is used.

Finally, additional tests were performed for the "large scale" surface with an increased amplitude of 1.801λ (rms slope 0.18), and

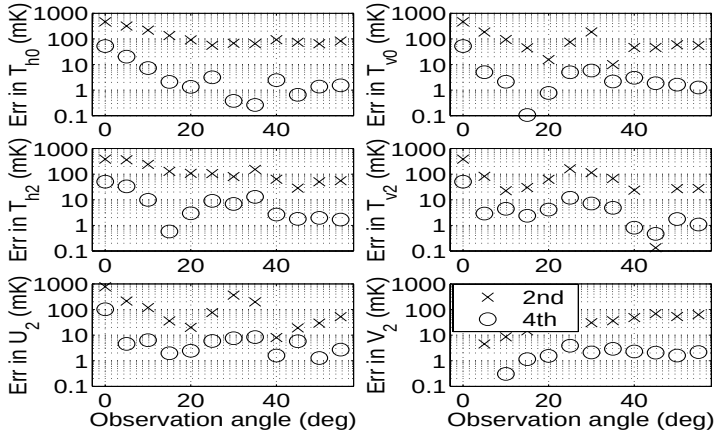

Figure 8. Error in T_{h0}, T_{v0}, T_{h2}, T_{v2}, U_2, and V_2 from second and fourth order SSA for bi-sinusoidal surface with $A = 0.072\lambda$, $P_x = 2.001\lambda$, and $P_y = 4.001\lambda$: $0^\circ < \theta < 55^\circ$.

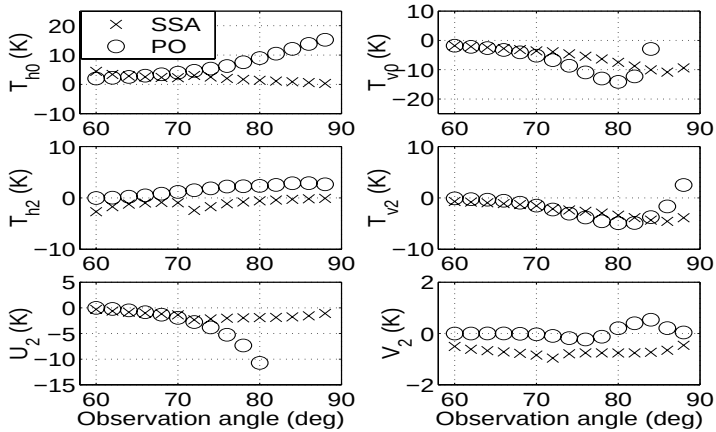

Figure 9. T_{h0}, T_{v0}, T_{h2}, T_{v2}, U_2, and V_2 for bi-sinusoidal surface with $A = 0.072\lambda$, $P_x = 2.001\lambda$, and $P_y = 4.001\lambda$ from twentieth order SSA and fourth order PO: $60^\circ < \theta < 89^\circ$.

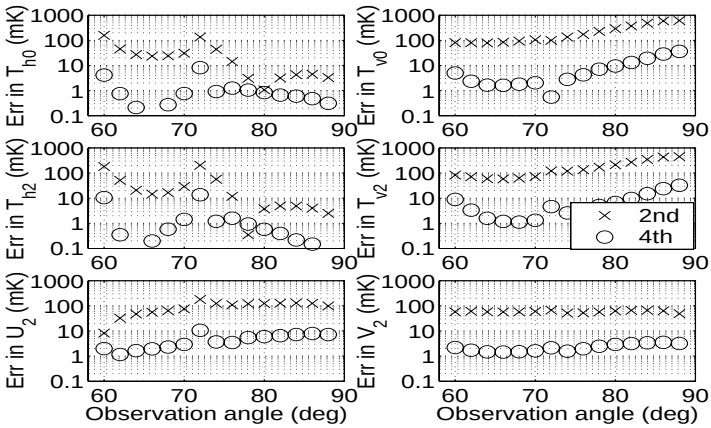

Figure 10. Error in T_{h0}, T_{v0}, T_{h2}, T_{v2}, U_2, and V_2 from second and fourth order SSA for bi-sinusoidal surface with $A = 0.072\lambda$, $P_x = 2.001\lambda$, and $P_y = 4.001\lambda$: $60^\circ < \theta < 89^\circ$.

for the "small scale" surface with an increased amplitude of 0.144λ (rms slope 0.3). Convergence of the higher-order SSA series degrades with the "large scale" surface amplitude, limiting the results that could be obtained with a quadruple precision code (twenty-sixth order) to the 1.801λ amplitude case. Results for the "large scale" surface in this case were very similar to those reported in Figures 2–6, although a moderately increased level of error in the second and fourth order methods was observed. In the "small scale" surface case, convergence of the SSA series remained rapid even with the surface amplitude doubled to 0.144λ, and the second and fourth order theories provided highly accurate predictions. These results demonstrate that the convergence of the SSA method for a given bi-sinusoidal surface slope depends strongly on the length scale of the surface considered, with performance degrading for larger length scale surfaces particularly at larger observation angles. Note that the rms slope value of 0.18 considered in the large scale surface case is likely greater than the rms slope of the "long wave" portion of the sea surface at wind speeds less than approximately 15 m/s for radiometers operating at 19 GHz.

5. CONCLUSIONS

The results of this study demonstrate that higher order implementations of the SSA and PO theories can provide improved predictions of the polarimetric brightness temperature of a rough surface. The

SSA theory was found to capture both the "large scale" and "short scale" surface brightnesses accurately, although the standard second order theory obtained some appreciable errors even for these relatively moderate slope surfaces at larger observation angles. These errors were typically reduced by the fourth order SSA, except for cases at larger observation angles with the large scale surface, where convergence of the SSA series appears slower. Convergence of the SSA series was found to depend strongly on the surface length scale considered, with more rapid convergence obtained with shorter length scale bi-sinusoidal surfaces. Standard (first order) PO predictions were found very accurate for the large scale surface at small to moderate observation angles, but to lose accuracy as multiple scattering and shadowing effects increased. Higher order multiple scattering terms in the PO series provided improved accuracy as long as shadowing effects remained insignificant, but larger errors were observed when shadowing effects became important. The V_2 parameter was inaccurately predicted by the higher PO theory as well, even in the large scale case when shadowing was not appreciable. PO predictions in the small scale surface case were found inaccurate due to the neglect of diffraction effects in the theory.

These results suggest that the PO theory can be regarded as highly accurate and efficient for "large scale" contributions alone to emitted power, but should be used with caution if small scale effects are believed important and if multiple scattering and shadowing effects are possible. Higher order corrections to the PO theory can provide some increased accuracy so long as shadowing effects are not appreciable, but the binary shadowing model used eventually produces significant errors. The fourth order SSA theory should be pursued for improving predictions in the multi-scale sea surface case, but care should still be used in interpreting fourth order predictions when large scale surface shadowing and multiple scattering may occur. A fourth order SSA theory should be analytically tractable following the procedures described in [22, 32], so that insight into multi-scale surface predictions can be obtained and relatively efficient implementations developed for use in practice. The higher order SSA numerical code described here also can be extended for use in multi-scale sea surface studies for a validation of fourth order predictions, although computational requirements will be increased as the range of length scales of interest increases. Because the commonly applied "two-scale" model of sea surface emission can be represented in terms of a PO model for large scale contributions combined with a "tilted" second order SSA theory for short scale contributions, further developments with the fourth order SSA theory will also play a role in improved assessment of the accuracy and limitations of the two-scale theory.

ACKNOWLEDGMENT

This work was sponsored by ONR contract N00014-00-1-0399. Use of the IBM SP system at the Maui High Performance Computing Center is acknowledged, sponsored by the Air Force Research Laboratory, Air Force Materiel Command under agreement F29601-93-2-0001. Opinions, interpretations, conclusions, and recommendations are those of the authors and are not necessarily endorsed by the United States Air Force, Air Force Research Laboratory, or the U.S. Government.

REFERENCES

1. Stogryn, A., "The apparent temperature of the sea at microwave frequencies," *IEEE Trans. Ant. Prop.*, Vol. 15, 278–286, 1967.
2. Wu, S. T. and A. K. Fung, "A noncoherent model for microwave emissions and backscattering from the sea surface," *J. of Geophys. Res.*, Vol. 77, 5917–5929, 1972.
3. Wentz, F. J., "A two-scale scattering model for foam-free sea microwave brightness temperatures," *J. Geophys. Res.*, Vol. 80, 3441–3446, 1975.
4. Etkin, V. S., N. N. Vorsin, Yu. A. Kravtsov, V. G. Mirovskii, V. V. Nikitin, A. E. Popov, and I. A. Troitskii, "Critical phenomena with the thermal radio irradiation of a periodically uneven water surface," *Izvestiya: Radiophysics and Quantum Electronics*, Vol. 21, 316–318, 1978.
5. Tsang, L. and J. A. Kong, "Energy conservation for reflectivity and transmissivity at a very rough surface," *J. Appl. Phys.*, Vol. 51, 673–680, 1980.
6. Tsang, L. and J. A. Kong, "Asymptotic solution for the reflectivity of a very rough surface," *J. Appl. Phys.*, Vol 51, 681–690, 1980.
7. Tsang, L., J. A. Kong, and R. T. Shin, *Theory of Microwave Remote Sensing*, Wiley, New York, 1985.
8. Irisov, V. G., I. G. Trokhimovskii, and V. S. Etkin, "Radiothermal spectroscopy of the sea-surface," *Doklady Akademii Nauk SSSR*, Vol. 297, 587–589, 1987.
9. Mikhailova, D. V. and I. M. Fuks, "Emissivity of a statistically rough surface including multiple reflections," *Sov. J. Commun. Tech. Elec.*, Vol. 38, 128–136, 1993.
10. Yueh, S. H., R. Kwok, F. K. Li, S. V. Nghiem, and W. J. Wilson, "Polarimetric passive remote sensing of ocean wind vectors," *Radio Science*, Vol. 29, 799–814, 1994.

11. Gasiewski, A. J. and D. B. Kunkee, "Polarized microwave emission from water waves," *Radio Science*, Vol. 29, 1449–1465, 1994.
12. Kunkee, D. B. and A. J. Gasiewski, "Simulation of passive microwave wind direction signatures over the ocean using an asymmetric-wave geometrical optics model," *Radio Science*, Vol. 32, 59, 1997.
13. Yueh, S. H., "Modeling of wind direction signals in polarimetric sea surface brightness temperatures," *IEEE Trans. Geosc. Remote Sens.*, Vol. 35, 1400–1418, 1997.
14. Irisov, V. G., "Small-slope expansion for thermal and reflected radiation from a rough surface," *Waves in Random Media*, Vol. 7, 1–10, 1997.
15. Johnson, J. T., R. T. Shin, and J. A. Kong, "Scattering and thermal emission from a two dimensional periodic surface," *Progress in Electromagnetic Research 15*, Chapter 11, J. A. Kong (ed.), EMW Publishing, Cambridge, Jan. 1997.
16. Camps, A., I. Corbella, and J. M. Rius, "Extension of Kirchhoff method under stationary phase approximation to determination of polarimetric thermal emission from the sea," *Electronics Letters,* Vol. 34, 1501–1503, 1998.
17. Johnson, J. T., R. T. Shin, L. Tsang, K. Pak, and J. A. Kong, "A numerical study of ocean polarimetric thermal emission," *IEEE Trans. Geosc. Remote Sens.*, Vol. 37, 8–20, 1999.
18. Johnson, J. T. and M. Zhang, "Theoretical study of the small slope approximation for ocean polarimetric thermal emission," *IEEE Trans. Geosc. Remote Sens.*, Vol. 37, 2305–2316, 1999.
19. Li, Q., L. Tsang, J. C. Shi, and C. H. Chan, "Application of physics based two-grid method and sparse matrix canonical grid method for numerical simulations of emissivities of soils with rough surfaces at microwave frequencies," *IEEE Trans. Geosc. Remote Sens.*, Vol. 38, 1635–1643, 2000.
20. Irisov, V. G., "Azimuthal variations of the microwave radiation from a slightly non-Gaussian sea surface," *Radio Science*, Vol. 53, 65–82, 2000.
21. Zhang, M. and J. T. Johnson, "Comparison of modeled and measured second azimuthal harmonics of ocean surface brightness temperatures," *IEEE Trans. Geosc. Remote Sens.*, Vol. 39, 448–452, 2001.
22. Johnson, J. T. and Y. Cai, "A theoretical study of sea surface up/down wind brightness temperature differences," to appear, *IEEE Trans. Geosc. Remote Sens.*, Jan. 2002.

23. Johnson, J. T., "Comparison of the physical optics and small slope theories for polarimetric thermal emission from the sea surface," accepted by *IEEE Trans. Geosc. Remote Sens.*, 2002.
24. Dzura, M. S., V. S. Etkin, A. S. Khrupin, M. N. Pospelov, and M. D. Raev, "Radiometers polarimeters: principles of design and applications for sea surface microwave emission polarimetry," *IGARSS 92 Conference Proceedings*, 1432–1434, 1992.
25. Wentz, F. J., "Measurement of oceanic wind vector using satellite microwave radiometers," *IEEE Trans. Geosc. and Remote Sens.*, Vol. 30, 960–972, 1992.
26. Yueh, S. H., W. J. Wilson, F. K. Li, S. V. Nghiem, and W. B. Ricketts, "Polarimetric measurements of sea surface brightness temperatures using an aircraft K-band radiometer," *IEEE Trans. Geosc. Remote Sens.*, Vol. 33, 85–92, 1995.
27. Gasster, S. D. and G. M. Flaming, "Overview of the conical microwave imager/sounder development for the NPOESS program," *IGARSS'98 Conference Proceedings*, Vol. 1, 268–271, 1998.
28. Yueh, S. H., W. J. Wilson, S. J. Dinardo, and F. K. Li, "Polarimetric microwave brightness signatures of ocean wind directions," *IEEE Trans. Geosc. Remote Sens.*, Vol. 37, 949–959, 1999.
29. Piepmeier, J. R. and A. J. Gasiewski, "High-resolution passive polarimetric microwave mapping of ocean surface wind vector fields," *IEEE Trans. Geosc. Remote Sens.*, Vol. 39, 606–622, 2001.
30. Klein, L. A. and C. T. Swift, "An improved model for the dielectric constant of sea water at microwave frequencies," *IEEE Trans. Ant. Prop.*, Vol. AP-25, 104–111, 1977.
31. Yueh, S. H., R. Kwok, and S. V. Nghiem, "Polarimetric scattering and emission properties of targets with reflection symmetry," *Radio Science*, Vol. 29, 1409–1420, 1994.
32. Johnson, J. T., "Third order small perturbation method for scattering from dielectric rough surfaces," *J. Opt. Soc. Am. A.*, Vol. 16, 2720–2736, 1999.
33. Johnson, J. T., "Erratum: Third order small perturbation method for scattering from dielectric rough surfaces," *J. Opt. Soc. Am. A.*, Vol. 17, 1685, 2000.
34. Bruno, O. P. and F. Reitich, "Numerical solution of diffraction problems: a method of variation of boundaries: III. Doubly periodic gratings," *J. Opt. Soc. Am. A.*, Vol. 10, 2551–2562, 1993.
35. *Maui High Performance Computing Center World Wide Web*

Site, on the World Wide Web at *www.mhpcc.edu*.

36. Press, W. H., S. A. Teukolsky, W. T. Vetterling, and B. P. Flannery, *Numerical Recipes: The Art of Scientific Computing*, second edition, Cambridge Univ. Press, New York, 1992.
37. Barrick, D. E., "Near grazing illumination and shadowing of rough surfaces," *Radio Science*, Vol. 30, 563–580, 1995.
38. Holliday, D., "Resolution of a controversy surrounding the Kirchhoff approach and the small perturbation method in rough-surface scattering theory," *IEEE Trans. Ant. Prop.*, Vol. 35, 120–122, 1987.
39. Fung, A. K., *Microwave Scattering and Emission Models and Their Applications*, Artech House, Norwood, MA, 1994.
40. Elfouhaily, T., D. R. Thompson, D. Vandemark, and B. Chapron, "A new bistatic model for electromagnetic scattering from perfectly conducting random surfaces," *Waves in Random Media*, Vol. 9, 281–294, 1999.
41. Garcia, N., V. Celli, N. Hill, and N. Cabrera, "Ill conditioned matrices in the scattering of waves from hard corrugated surfaces," *Phys. Rev. B.*, Vol. 18, 5184–5189, 1978.
42. Blackford, L. S., J. Choi, A. Cleary, E. D'Azevedo, J. Demmel, I. Dhillon, J. Dogarra, S. Hammarling, G. Henry, A. Petitet, K. Stanley, D. Walker, and R. C. Whaley, *Scalapack Users' Guide*, SIAM Publications, Philadelphia, 1997.